Interface Damage Model for Thermomechanical Degradation of Heterogeneous Materials *

K. Willam, I. Rhee & B. Shing
University of Colorado at Boulder, USA

ABSTRACT: In this paper we examine the degradation of interface transition zones in heterogeneous materials due to thermal and mechanical damage. After a brief introduction of zero-thickness interface models, we will address three topics, (a) the interaction of normal and tangential damage at the interface level of observation, (b) the interaction of thermal and mechanical damage when thermal softening is coupled with mechanical degradation, and (c) the effect of interface damage on the load resistance of heterogeneous composites such as concrete when thermal softening leads to massive degradation of their load resistance.

1 INTRODUCTION

Ever since Charles A. Coulomb articulated the classical law of dry friction over 200 years ago, a precise mathematical description of material interface behavior has been one of the central themes in engineering mechanics and materials. Interfaces are normally the weak link in heterogeneous media. A successful predictive model will have enormous implications for design, analysis, fabrication, and life cycle performance of multi-material structures. It also has a strategic role in capturing discontinuous failure processes in materials which are considered homogeneous at the macroscale. The main problem is that current interface models are calibrated not directly but indirectly by inverse identification since no established theory exists how to construct zero-thickness interface properties from micro-structural features of the adherent materials.

Interface adhesion, cohesion and friction are important in many technological realms ranging from the scales of kilometers in geosciences to micro- and nanometers in microelectronics and nano device applications. In all cases, computationally-efficient modeling strategies are lacking that pass information between lower and higher length scales and thus facilitate the rational analysis and design of engineering systems. In the back of these fundamental issues on multiscale analysis and design of material systems is the field of material failure where degradation of material interfaces play a central role in multi-materials under extreme events. Specifically, this paper will examine high temperature effects on heterogeneous materials and the fields of fire protection and fire resistance of cement-based materials. Thereby, the exploratory study is intended as a proof of concept for multi-scale multi-physics engineering to reduce ablation and spall effects in thermal shock problems when fire safety issues are considered.

*accepted for publication in Special WCCMV Issue on Computational Failure Mechanics in CMAME, 2003

2 SCOPE

In the paper we examine thermal and mechanical deterioration effects of interfacial transition zones in heterogeneous two-phase materials such as concrete. After a brief introduction we consider special forms of damage in zero-thickness interface models. To this end we present a systematic discussion of normal and tangential interface damage and their interaction as well as the coupling of elastic and thermal degradation when heat transfer takes place in a heterogeneous material system subject to strong discontinuities along some of the interfaces. For illustration the thermal degradation formulation is applied to model-based simulations of two-phase composites considering a single inclusion problem and the thermal sweep analysis of a two-phase particle composite. The first application shows the effects of degradation when thermo-mechanical mismatch of the two-phase material introduces localized degradation at the interfaces between the constituents. The second application is motivated by experimental observations on concrete specimens that were subjected to the combined thermal and mechanical load histories leading to overall degradation of load resistance during thermal sweeps.

3 BACKGROUND

Traditionally, material interfaces are considered to exhibit tensile bond and shear resistance at the macroscopic continuum level. While in most applications this approach may be adequate, progressive decohesion processes can only be explained properly by considering micro-structural details at the interface. This requires characterization of the two adherent constituents and the interface bond conditions. These types of studies are very demanding in terms of manpower and computing power, in spite of the recent development of high performance modeling of materials at the micro- and macroscopic levels in 3-D space and time.

3.1 *Zero-Thickness Interface Behavior*

The notion of a zero-thickness interface results in elastic stiffness properties which relate surface tractions to relative displacements. In 2-D the normal and tangential shear components lead in local coordinates to the elementary stiffness relationship,

$$\left[\begin{array}{c} t_n \\ t_s \end{array}\right] = \left[\begin{array}{cc} k_{nn} & 0 \\ 0 & k_{ss} \end{array}\right] \left[\begin{array}{c} \Delta u_n \\ \Delta u_s \end{array}\right] \tag{1}$$

Thereby it is understood that the relative displacements are discontinuous across the zero-thickness interface. In other terms we should write $\Delta u_n = u_n^+ - u_n^- = [|u_n|]$ and $\Delta u_s = u_s^+ - u_s^- = [|u_s|]$. Considering an interfacial transition zone of the thickness ℓ_{el} we may interpret the relative displacements as normal strain and shear strain, where $\Delta u_n = \epsilon_n \, \ell_{el}$ and $\Delta u_s = \gamma_{ns} \, \ell_{el}$. Consequently, the elastic finite thickness interface relation results in,

$$\left[\begin{array}{c} t_n \\ t_s \end{array}\right] = \left[\begin{array}{cc} E & 0 \\ 0 & G \end{array}\right] \left[\begin{array}{c} \epsilon_n \\ \gamma_{ns} \end{array}\right] \tag{2}$$

This implies that zero-thickness interface stiffness properties are related to the elastic moduli of elasticity by,

$$k_{nn} = E/\ell_{el} \quad \text{and} \quad k_{ss} = G/\ell_{el} \tag{3}$$

This asymptotic argument illustrates the fundamental role of the elastic interface thickness ℓ_{el}. Its purpose is to account for the dimensional reduction when we map the elastic moduli of the bulk material onto zero-thickness interface properties with the help of the length scale ℓ_{el}. Aside from the dimensional

reduction process of volume vs surface dominated energy arguments, the elastic interface stiffness provides the repository for elastic damage when tensile separation and shear slip are considered in terms of a surface dominated degradation process governed by constant fracture energy release rates G_c^I and G_c^{II}, in mode I and mode II (as well as G_c^{III} in Mode III in 3-D). Thereby, the volume dominated degradation process is transformed into a surface dominated fracture process. The dimensional reduction localizes degrading softening phenomena to the interface surface thereby regularizing the failure process with regard to fracture energy release rate. The role of the interface is to trap the formation of large gradients in the continuum into a discontinuous interface similarly to *'wall-laws'* in fluid-structure interaction problems.

3.2 *Elastic Interface Damage Based on Two Damage Variables*

The nature of material interfaces is inherently local when the strong kinematic discontinuities of zero-thickness interfaces are considered. Conceptually, there are two points of view possible:

(a) the interface properties are projections of the adherent material bulk properties. This concept is normally adopted in embedded crack methodologies where localization of kinematic discontinuities leads to an appropriate dimensional reduction of the bulk properties, see Simo, Oliver and Armero [1993], Oliver, Huespe, Pulido and Chaves [2001].

(b) the interface properties have a life of their own, Rots & Schellekens [1990], Stankowski, Runesson and Sture [1993], Lofti & Shing [1994], Carol, Prat and Lopez [1997]. The interfacial transition zone of bimaterials are an example where the thickness is normally so small that it may be assumed to be zero when compared to the scale of adjacent bulk materials. This concept is normally adopted for the formulation of joint elements, fictitious crack models and zero-thickness cohesion models, see Xu & Needleman [1994], Camacho & Ortiz [1996] and Espinosa & Zavattieri [2003], which have been motivated by binding forces at the atomistic level.

In what follows we adopt the latter philosophy with focus on zero-thickness interface elements for decohesion and frictional slip based on microstructural features of the adherent materials. The *'Fictitious Crack Approach'* of Hillerborg, Modeer and Petersson [1976] is well established to formulate the loss of cohesion in a zero-thickness bond layer in mode I. An additional aspect of constitutive interface modeling arises when we consider the geometry of contact surfaces which is rarely smooth and planar, but full of asperities providing localized points of contact. Consequently, the classical interpretation of continuum damage mechanics of Kachanov [1958] is highly appropriate, where the effective load bearing area provides the skeleton for stress transfer as opposed to the nominal surface area, $1 - d = A_{eff}/A_{nom}$ with $0 \leq d \leq 1$. In this context, the *'Disturbed State Concept'* of Desai [2001] introduced some innovative but still intuitive ideas to the field of interface modeling.

Although the thermodynamic setting of interface constitutive models is not well established, one can start from the postulate that there exists a free surface energy in the spirit of Helmholtz. There are a number of issues related to the *'coupling'* effects when dissipative interface processes are subjected to decohesion and frictional slip in a transient thermomechanical environment. For illustration we consider the free Helmholtz energy format in a 2-D setting omitting for the time being thermal and inelastic dissipation effects for the sake of argument.

Redefining the specific free surface energy per unit mass in terms of a potential per unit surface, then additive expansion of damage in the normal and tangential energy components,

$$\Psi([|u_n|],[|u_s|],d_n,d_s)=\frac{1}{2}[1-d_n]k^o_{nn}[|u_n|]^2+\frac{1}{2}[1-d_s]k^o_{ss}[|u_s|]^2 \tag{4}$$

yields the normal and tangential interface tractions :

$$t_n=\frac{\partial\Psi}{\partial[|u_n|]}=[1-d_n]k^o_{nn}[|u_n|] \quad \text{and} \quad t_s=\frac{\partial\Psi}{\partial[|u_s|]}=[1-d_s]k^o_{ss}[|u_s|] \tag{5}$$

and the thermodynamic conjugate forces :

$$\mathcal{Y}_n=-\frac{\partial\Psi}{\partial d_n}=\frac{1}{2}k^o_{nn}[|u_n|]^2 \quad \text{and} \quad \mathcal{Y}_s=-\frac{\partial\Psi}{\partial d_s}=\frac{1}{2}k^o_{ss}[|u_s|]^2 \tag{6}$$

The mechanical dissipation inequality for isothermal conditions,

$$\dot{\mathcal{D}}_m=\mathcal{Y}_n\dot{d}_n+\mathcal{Y}_s\dot{d}_s\geq 0 \tag{7}$$

is satisfied as long as the damage parameters are monotonically increasing functions, $\dot{d}_n>0$ and $\dot{d}_s>0$, since the thermodynamic forces $\mathcal{Y}_n,\mathcal{Y}_s$ are strictly positive.

Introducing two independent damage functions,

$$F_n=\mathcal{Y}_n-r_n(d_n)\leq 0 \quad \text{and} \quad F_s=\mathcal{Y}_s-r_s(d_s)\leq 0 \tag{8}$$

the internal energy demand due to the load is expressed in terms of the thermodynamic forces $\mathcal{Y}_n,\mathcal{Y}_s$, and the resistance by the scalar function of the damage variable, $r(d_n),r_s(d_s)$. Under persistent damage in the normal and tangential components the two consistency conditions,

$$\dot{F}_n=\frac{\partial F_n}{\partial\mathcal{Y}^n}\dot{\mathcal{Y}}_n+\frac{\partial F_n}{\partial d_n}\dot{d}_n=0 \quad \text{and} \quad \dot{F}_s=\frac{\partial F_s}{\partial\mathcal{Y}^s}\dot{\mathcal{Y}}_s+\frac{\partial F_s}{\partial d_s}\dot{d}_s=0 \tag{9}$$

yield the evolution equations of normal and tangential damage:

$$\dot{d}_n=\frac{1}{\mathcal{H}_n}t^{eff}_n\langle[|\dot{u}_n|]\rangle \quad \text{where} \quad t^{eff}_n=k^o_{nn}[|u_n|] \quad \text{and} \quad \dot{d}_s=\frac{1}{\mathcal{H}_s}t^{eff}_s[|\dot{u}_s|] \quad \text{where} \quad t^{eff}_s=k^o_{ss}[|u_s|] \tag{10}$$

where the hardening/softening parameters $\mathcal{H}_n,\mathcal{H}_s$ characterize the rate of damage evolution of the normal and tangential interface properties. The hardening/softening moduli, $\mathcal{H}_n,\mathcal{H}_s$, define the rate of change of degradation of the cohesive properties in tension and shear which may be expressed by an exponential function of the damage variable leading to the traction relation illustrated in Figure 1.

In what follows, normal damage is considered to be a unilateral process of crack closure. It is active only in tension but not in compression inferred by the Macaulay brackets, $\langle[|\dot{u}_n|]\rangle$, used to activate positive values of interface opening in the normal direction.

Differentiating the constitutive relationship of interface tractions,

$$\begin{bmatrix} t_n \\ t_s \end{bmatrix}=\begin{bmatrix} [1-d_n]k^o_{nn} & 0 \\ 0 & [1-d_s]k^o_{ss} \end{bmatrix}\begin{bmatrix} \langle[|u_n|]\rangle \\ [|u_s|] \end{bmatrix} \tag{11}$$

leads to the tangential traction relationship,

$$\begin{bmatrix} \dot{t}_n \\ \dot{t}_s \end{bmatrix}=\mathbb{k}^{tan}_{ed}\begin{bmatrix} \langle[|\dot{u}_n|]\rangle \\ [|\dot{u}_s|] \end{bmatrix} \tag{12}$$

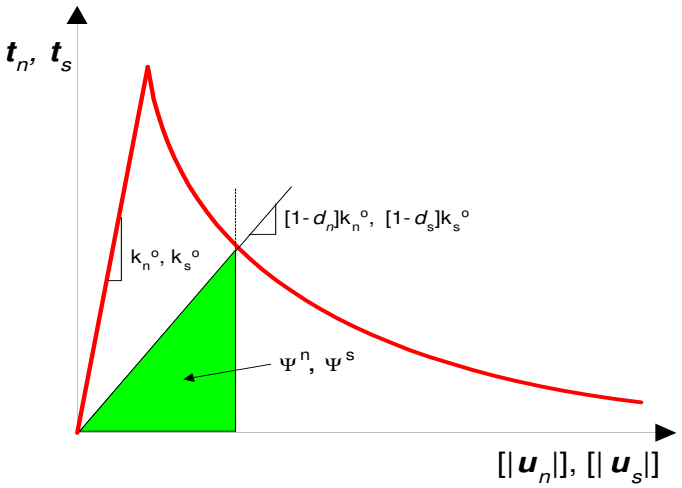

Figure 1: Schematics of free energy release due to cohesive degradation

where the tangential elastic damage stiffness reads,

$$\mathbb{k}_{ed}^{tan} = \begin{bmatrix} [1-d_n]k_{nn}^o & 0 \\ 0 & [1-d_s]k_{ss}^o \end{bmatrix} - \begin{bmatrix} \frac{1}{\mathcal{H}_n} t_n^{eff} t_n^{eff} & 0 \\ 0 & \frac{1}{\mathcal{H}_s} t_s^{eff} t_s^{eff} \end{bmatrix} \tag{13}$$

Note the decoupling of the normal and shear components in the tangential stiffness relation if two independent damage variables are used without interaction.

3.3 *Coupling of Normal-Tangential Interface Damage*

In what follows let us consider coupling between the two damage processes in the form of a single damage mechanism. Assuming isotropic interface stiffness properties, $k^o = k_{nn}^o = k_{ss}^o$, we recognize the physical meaning of the thermodynamic force as fracture energy release rates in mode I and mode II we consider the normalized interaction relation in 2-D,

$$[(\frac{\mathcal{Y}_n}{G_c^I})^a + (\frac{\mathcal{Y}_s}{G_c^{II}})^a]^{\frac{1}{a}} = 1 \tag{14}$$

This format suggests that we introduce an equivalent thermodynamic force which corresponds to the critical fracture energy release rate in mode I, $\mathcal{Y}_{eq} = G_c^I$. Letting $a = 1$ for the sake of simplicity we find,

$$\mathcal{Y}_{eq} = \mathcal{Y}_n + b\mathcal{Y}_s = \frac{1}{2} k^o \left[\langle [|u_n|]^2 \rangle + b \, [|u_s|]^2 \right] \quad \text{where} \quad b = \frac{G_c^I}{G_c^{II}} \tag{15}$$

The fracture energy ratio b defines the relationship of the critical fracture energy release rates in mode I and in mode II. This type of interaction relation was originally proposed by Brewer-Lagace [1988] and adopted for delamination analysis by Corigliano and Allix [2000]. A similar approach was adopted by Carol, Rizzi and Willam [2002] for introducing volumetric-deviatoric components in terms of single damage variable in an otherwise orthotropic damage model.

As noted above, the reduced dissipation inequality in Equation 7 is satisfied as long as the damage variables are monotonically increasing functions since the thermodynamic forces are strictly positive. Constraining the normal and tangential degradation in terms of a single scalar damage variable, $d = d_n = b\, d_s$, the dissipation inequality reduces to the compact form,

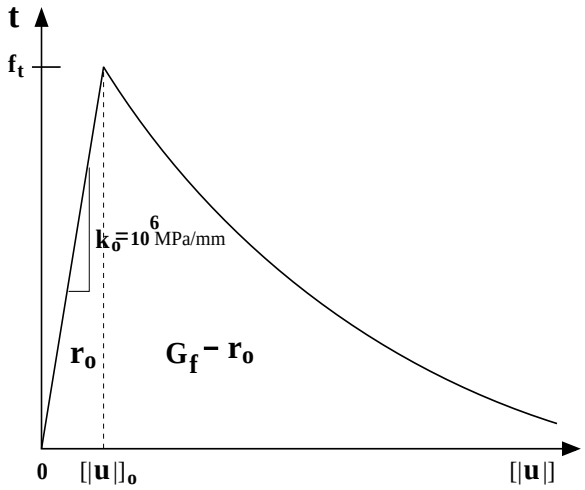

Figure 2: Fracture energy-based separation law of interface traction

$$\dot{\mathcal{D}}_m = \mathcal{Y}_n \dot{d}_n + \mathcal{Y}_s \dot{d}_s = \mathcal{Y}_{eq} \dot{d} \geq 0 \tag{16}$$

In this case the evolution of scalar damage is activated by the single damage function,

$$F_d = \mathcal{Y}_{eq} - r(d) = 0 \tag{17}$$

Thus, under persistent loading the consistency condition, $\dot{F}_d = 0$, furnishes the rate of damage,

$$\dot{d} = \frac{\dot{\mathcal{Y}}_{eq}}{\mathcal{H}_d} = \frac{1}{\mathcal{H}_d} \left[t_n^{eff} \langle [|\dot{u}_n|] \rangle + b\, t_s^{eff} [|\dot{u}_s|] \right] \quad \text{where} \quad \mathcal{H}_d = -\frac{\partial F_d}{\partial d} = \frac{\partial r(d)}{\partial d} \tag{18}$$

The hardening function $\mathcal{H}_d$ is calibrated from mode I decohesion experiments conceptually shown in Figure 2.

Introducing damage in the form of an exponential function,

$$d = 1 - \sqrt{\frac{r_o}{r}} e^{\gamma(1-\sqrt{\frac{r}{r_o}})} \tag{19}$$

where, $\gamma = \frac{2r_o}{G_f - r_o}$, $r_o = \frac{1}{2} k^o [|u_o|]^2$, $r = \frac{1}{2} k^o [|u|]^2$, then the tangential relation reads:

$$\dot{t} = (1-d) k^o [|\dot{u}|] - \dot{d} t_{eff} \tag{20}$$

where, $\dot{d} = \frac{\partial d}{\partial r} \frac{\partial r}{\partial [|u|]} = \frac{1}{\mathcal{H}_d} t_{eff} [|\dot{u}|]$, with $\frac{1}{\mathcal{H}_d} = \frac{\partial d}{\partial r}$, and $\frac{\partial r}{\partial [|u|]} = t_{eff} [|\dot{u}|]$. In this case the hardening/softening damage law is described by,

$$\frac{1}{\mathcal{H}_d} = \frac{r_o e^{\gamma(1-\sqrt{\frac{r}{r_o}})}}{2r^2 \sqrt{\frac{r_o}{r}}} + \frac{\gamma\, e^{\gamma(1-\sqrt{\frac{r}{r_o}})} \sqrt{\frac{r_o}{r}}}{2r_o \sqrt{\frac{r}{r_o}}} \tag{21}$$

In summary, the evolution law involves three parameters, the elastic interface stiffness $k^o = E/\ell_{el}$, the cohesive strength f_t, and through the exponential softening parameter γ the fracture energy release rate G_f^I in mode I. They determine the resistance in terms of the elastic surface energy at crack initiation, r^o, and the exponential softening response due to damage thereafter.

The tangential stiffness properties result from differentiation of the interface traction relations in Equation 11,

$$\mathbb{k}^{tan} = \frac{1}{2}[1-d]\frac{\partial^2 \psi_o}{\partial[|u_n|] \otimes \partial[|u_s|]} - \frac{\dot{d}}{1-d}\mathbf{t}_{eff} \tag{22}$$

In expanded form this results in the tangential stiffness for elastic damage,

$$\mathbb{k}_{ed}^{tan} = \begin{bmatrix} [1-d]k^o & 0 \\ 0 & [1-d]k^o \end{bmatrix} - \frac{1}{\mathcal{H}_d}\begin{bmatrix} t_n^{eff}t_n^{eff} & b[t_n^{eff}t_s^{eff}] \\ b[t_s^{eff}t_n^{eff}] & b^2[t_s^{eff}t_s^{eff}] \end{bmatrix} \tag{23}$$

which is symmetric as opposed to the formulation proposed by Tijssens [2000]. The coupled format should be compared with the uncoupled format in Equation 13 which involves the two independent damage variables $[1-d_n]$ and $[1-d_s]$. It might be surprising that the simple format of a single scalar damage variable leads to the coupled format above. However, the interaction of normal and tangential damage properties in the tangential format simply reflects the nonlinearity during loss of cohesion, whereby, the single damage variable $[1-d]$ introduces the interaction among normal and tangential damage.

3.4 *Computational Aspects*

Beside the challenge of capturing the main features of interface behavior, there are several significant mathematical issues which are central to this paper and the entire field of interface analysis.

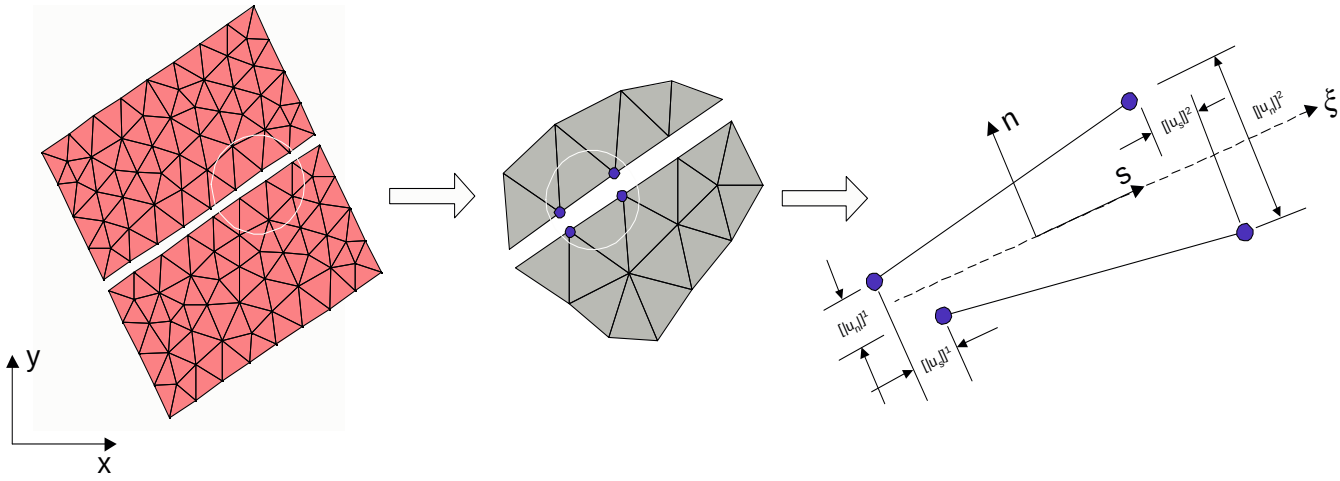

Figure 3: Zero-thickness interface element strategy

For the sake of argument let us consider the linear case in which the inter-element stiffness contributions play the role of penalty functions to enforce adherence among the two subdomains shown in Figure 3. In physical terms, the stiffness assembly is comprised of disconnected solid elements which are interacting through interface elements. Consequently the interface stiffness properties must not only be sufficiently large to remove rigid body modes of the connected material structure, but they must also minimize displacement discontinuities among adherent solid elements during initially intact conditions. This is achieved by values of the interface stiffness which are normally three orders of magnitude larger than the bulk stiffness in order to separate the low frequency content of the bulk behavior from the high frequency content of the interface elements. In other terms, the elastic length scale of the dimensional reduction infers that the physical dimension of the interface thickness is three orders of magnitude smaller

than that of the adherent solid domain. Considering degradation of the thickness of the elastic interface is initially $\ell_{el} = \frac{E}{[1-d]k^o} \sim 10^{-3}$ in the appropriate length units when $d = 0$. For increasing damage the elastic length scale, or in other terms, the width of the interface increases as $d \to 1$.

In this context we should be aware that Irwin's characteristic dimension $\ell_{ch} = \frac{E\,G_c}{(f_t)^2}$ is a measure of the length of the fracture process zone, Hillerborg et al [1976]. In quasi-brittle materials this length scale is sufficiently small such that fracture initiation and propagation is governed by the stress intensity factor at the crack tip. In cement-based materials typical values are in the range of $\ell_{ch} \sim 10^3\,[mm]$, partly because of the heterogeneous nature of concrete materials with aggregate sizes in the range of $10 - 100\,[mm]$. This strongly suggests that self-similarity arguments for crack propagation are no longer valid and that concrete fracture is a NLFM process governed by decohesion and loss of frictional resistance in the interfacial transition zones. In fact, considering the elastic interface length scale above, $\ell_{el} = \frac{E}{[1-d]k^o}$, we can correlate the two length scales in the form $\ell_{ch} = \beta\ell_{el}$, where $\beta = \frac{[1-d]k^o\,G_c}{(f_t)^2}$. For concrete materials this length ratio initially is in the range $\beta \sim 10^5$ when $d = 0$. During progressive degradation, as the 'fictitious crack' widens the ratio of the fracture process zone $\beta = \frac{\ell_{ch}}{\ell_{el}}$ decreases as $d \to 1$. In other terms, the degradation of the cohesive-frictional process zone is emulated quite realistically in the interface layer of zero-thickness.

Aside from the modeling aspects of interface computations there is also an exciting theoretical aspect which changes the normal conformity arguments of *'compatible'* finite element displacement methods. This is the field of *'Discontinuous Galerkin Methods'* which has received considerable attention by the mathematically-oriented finite element community. In this case the discretization of bulk elements is freed from conformity arguments when displacement as well as traction continuity is enforced by Lagrange multipliers.

On the numerical side, there are issues of interdependent interpolation when we consider the variation of interface tractions and the variation of bulk stresses in adherent solid elements, see Gens, Carol and Alonso [1990] and Schellekens & de Borst [1993]. Using conforming displacement expansions for the interface and adherent solid elements, it is apparent that the variation of interface tractions is of higher order than the variation of stresses in neighboring solid elements. Consequently, provisions have to made to suppress oscillations in the interface traction field. In our case of linear interpolants, Lobatto integration is used which results in interface stiffness properties which turn out to be diagonal (including the coupling partitions) if a natural numbering of nodes is used.

4 THERMOMECHANICAL MODEL OF INTERFACE DAMAGE

The zero-thickness interface transition zone is illustrated in Figure 4, where the jumps in the normal and tangential displacement introduce the kinematic discontinuities,

$$[|\mathbf{u}|] = \mathbf{u}^+ - \mathbf{u}^- \neq 0 \quad \text{and} \quad [|\mathbf{t}|] = \mathbf{t}^+ - \mathbf{t}^- = \mathbf{0} \tag{24}$$

while the interface tractions are assumed to remain continuous. Moreover, we assume that the temperature field will develop jump conditions across the interface due to strong discontinuities of the interface kinematics.

$$[|\Delta T|] = T^+ - T^- \neq 0 \tag{25}$$

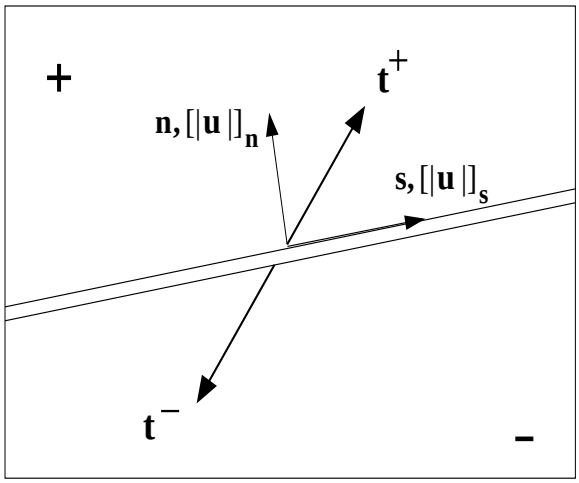

Figure 4: Mechanical jump conditions across zero-thickness interface

4.1 *Free Energy Potential for Thermoelastic Interface Damage*

In what follows we introduce the effect of temperature in the elastic damage formulation. To this end we consider the free energy potential to be a function of the discontinuous interface displacements, $[|u_n|], [|u_s|]$, the temperature jump across the interface, $[|\Delta T|] = [|T - T_o|]$, and the single damage variable d,

$$\boxed{\Psi = \Psi([|u_n|], [|u_s|], [|\Delta T|], d)} \tag{26}$$

For definiteness, we expand the free surface energy into a quadratic polynomial in the primal variables with the understanding that the nonlinear mechanical and thermal response will be embedded in the thermomechanical damage variable d :

$$\Psi = g_0 [|\Delta T|] + g_1 [|u_n|] + g_2 [|u_s|] + \frac{1}{2} g_3 [|u_n|]^2 + \frac{1}{2} g_4 [|u_s|]^2 + \tag{27}$$

$$g_5 [|u_n|] [|u_s|] + g_6 [|u_n|] [|\Delta T|] + g_7 [|u_s|] [|\Delta T|] - \frac{1}{2} c_s [|\Delta T|]^2 \tag{28}$$

Hereby, the response functions $g_i = g_i(d)$ are functions of the thermomechanical damage variable $1 - d = [1 - d_u][1 - d_T]$, while c_s denotes the heat capacity per unit surface area.

The gradients of the surface energy potential with regard to the displacement jumps furnish the nominal interface tractions,

$$\mathbf{t} = [1 - d] \frac{\partial \Psi}{\partial [|\mathbf{u}|]} \tag{29}$$

which read in component form :

$$t_n = g_1 + g_3 [|u_n|] + g_5 [|u_s|] + g_6 [|\Delta T|] \tag{30}$$

$$t_s = g_2 + g_4\,[|u_s|] + g_5\,[|u_n|] + g_7\,[|\Delta T|] \tag{31}$$

For the sake of argument we assume isotropic interface behavior, where the damage interface stiffness $g_3 = g_4 = [1-d]k^o$, and where the initial thermal stress is the same in the normal and tangential directions, $g_6 = g_7 = -[1-d]\alpha_s^o k^o$. Thereby, we understand that the coefficient of thermal surface expansion depends on the characteristic length, $\alpha_s^o = \alpha\,\ell_{el}$, because of the definition of the interface stiffness k^o. This assures consistent units similarly to the heat capacity per unit surface mass which is subject to thermomechanical damage, $c_s = [1-d]c$. Further, we omit initial interface tractions, $g_1 = g_2 = 0$, and we delete anisotropic coupling of the normal and tangential components in the interface jump conditions assuming $g_5 = 0$. In this case, the normal and tangential interface traction expressions reduce to,

$$t_n = [1-d]k^o\,[|u_{n,el}|] \quad \text{where} \quad [|u_{n,el}|] = [|u_n|] - \alpha_s^o\,[|\Delta T|] \tag{32}$$

$$t_s = [1-d]k^o\{[|u_{s,el}|] \quad \text{where} \quad [|u_{s,el}|] = [|u_s|] - \alpha_s^o\,[|\Delta T|] \tag{33}$$

In matrix form, the tractions are a linear map of the interface displacement and temperature jumps,

$$\left[\begin{array}{c} t_n \\ t_s \end{array}\right] = [1-d]\left[\begin{array}{cc} k^0 & 0 \\ 0 & k^0 \end{array}\right]\left[\begin{array}{c} [|u_n|] - \alpha_s^0\,[|\Delta T|] \\ [|u_s|] - \alpha_s^0\,[|\Delta T|] \end{array}\right] \tag{34}$$

which highlights the isotropic features of the thermoelastic damage model.

The thermodynamic conjugate forces follow the interaction relation between normal and tangential components developed in Equation 15. In this case the thermodynamic force $\mathcal{Y}_{eq}$ is equivalent to the fracture energy release rate for mode I fracture,

$$\mathcal{Y}_{eq} = -\frac{\partial \Psi}{\partial d} = \frac{1}{2}k^o\{[|u_{n,el}|]^2 + b\,[|u_{s,el}|]^2\} \quad \text{where} \quad b = \frac{G_c^I}{G_c^{II}} \tag{35}$$

4.2 *Clausius-Duhem Inequality*

Recalling the local form of the second law of continuum thermodynamics and writing the Clausius-Duhem inequality in terms of the Helmholtz free energy we find,

$$\boldsymbol{\sigma} : \dot{\boldsymbol{\epsilon}} - \rho\dot{\Psi} - \rho s\dot{\theta} - \tfrac{\mathbf{q}\cdot\nabla_x\theta}{\theta} \geq 0 \tag{36}$$

where s denotes the local entropy and θ the absolute temperature. A sufficient condition of the inequality may be expressed in terms of the modified dissipation inequality,

$$\dot{\mathcal{D}}^{mod} = \boldsymbol{\sigma} : \dot{\boldsymbol{\epsilon}} - \rho\dot{\Psi} - \rho\, s\dot{\theta} \geq 0 \tag{37}$$

when the contribution of the conduction inequality is strictly negative using the Fourier law, $\frac{\mathbf{q}\cdot\nabla_x\theta}{\theta} < 0$.

Forming the total differential of the free energy, $\dot{\Psi}$, and invoking the Coleman relations for the surface tractions, Equations 32, 33, a sufficient condition for mechanical dissipation may be developed in the reduced form in analogy to Equation 16,

$$\dot{\mathcal{D}}^{mech} = \mathcal{Y}_{eq}\,\dot{d} \geq 0 \tag{38}$$

Thereby, elastic interface damage is a function of the interface displacement jump, $d_u = 1 - \frac{k(u)}{k^o}$, and thermal damage is a function of the mean value of the temperature jump across the interface, $d_T = 1 - \frac{\alpha_s(\Delta T_{avg})}{\alpha_s^o}$. The combined damage factor is the product of thermal and mechanical damage,

$$[1-d] = [1-d_u][1-d_T] \quad \text{such that} \quad \dot{d} = \dot{d}_u[1-d_T] + \dot{d}_T[1-d_u] \tag{39}$$

The two-way coupling of mechanical and thermal degradation becomes more apparent if we consider the entropy,

$$s = -\frac{\partial \Psi}{\partial\,[|\Delta T|]} = -g_o + [1-d]\alpha_s^o k^o\,[|u_{n,el}|] + [1-d]\alpha_s^o k^o\,[|u_{s,el}|] + c_s[1-d]\,[|\Delta T|] \tag{40}$$

This raises the issue of positive entropy production which is satisfied only when $d \leq 1$ and $[|\dot{u}_{n,el}|] > 0$, $[|\dot{u}_{s,el}|] > 0$ and $\left[\left|\Delta \dot{T}\right|\right] > 0$, and when damage decreases for positive values of displacement and temperature jumps, $-\dot{d} > 0$.

4.3 *Rate Form of Interface Tractions*

The tangential damage relations are obtained from differentiating the traction expressions in Equation 34,

$$\dot{t}_n = [1-d]k^o\,[|\dot{u}_{n,el}|] - \dot{d}\,t_{n,el}^{eff} \quad \text{where} \quad t_{n,el}^{eff} = k^o\{[|u_{n,el}|] \tag{41}$$

$$\dot{t}_s = [1-d]k^o\,[|\dot{u}_{s,el}|] - \dot{d}\,t_{s,el}^{eff} \quad \text{where} \quad t_{s,el}^{eff} = k^o\{[|u_{s,el}|] \tag{42}$$

For persistent thermoelastic damage, the consistency conditions furnish the evolution law for the rate of mechanical damage in analogy to Equation 18,

$$\dot{d} = \frac{1}{\mathcal{H}_d}\dot{\mathcal{Y}}_{eq} = \frac{1}{\mathcal{H}_d}\{t_{n,el}^{eff}\langle[|\dot{u}_{n,el}|]\rangle + b\,t_{s,el}^{eff}[|\dot{u}_{s,el}|]\} \tag{43}$$

Consequently, the rate of normal and tangential interface tractions is driven by the rate of interface displacement and temperature jumps, such that

$$\boxed{\dot{\mathbf{t}} = \mathbb{k}_{ted}^{tan}\,[|\dot{\mathbf{u}}|] - \boldsymbol{\beta}_{ted}^{tan}\left[\left|\Delta\dot{\mathbf{T}}\right|\right]} \tag{44}$$

The tangential interface stiffness for elastic degradation expands into,

$$\mathbb{k}_{ted}^{tan} = [1-d]k^o\begin{bmatrix} 1 & 0 \\ 0 & 1 \end{bmatrix} - \frac{1}{\mathcal{H}_d}\begin{bmatrix} t_{n,el}^{eff}{t_{n,el}}^{eff} & b[t_{n,el}^{eff}t_{s,el}^{eff}] \\ b[t_{s,el}^{eff}t_{n,el}^{eff}] & b^2[t_{s,el}^{eff}t_{s,el}^{eff}] \end{bmatrix} \tag{45}$$

and the thermal interface tractions associated with the temperature rate read :

$$\boldsymbol{\beta}_{ted}^{tan} = -[1-d]\alpha_s^o k^o\begin{bmatrix} 1 & 0 \\ 0 & 1 \end{bmatrix} + \frac{\alpha_s^o}{\mathcal{H}_d}\begin{bmatrix} t_{n,el}^{eff}{t_{n,el}}^{eff} & b[t_{n,el}^{eff}t_{s,el}^{eff}] \\ b[t_{s,el}^{eff}t_{n,el}^{eff}] & b^2[t_{s,el}^{eff}t_{s,el}^{eff}] \end{bmatrix} \tag{46}$$

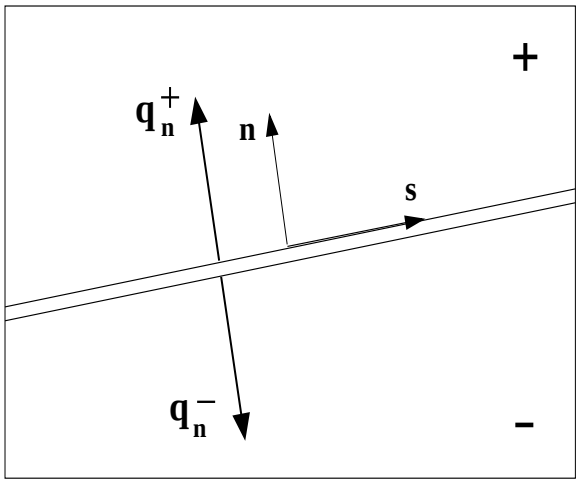

Figure 5: Thermal jump condition across zero-thickness interface

4.4 *Interface Heat Transfer*

The zero-thickness interface transition zone is illustrated in Figure 5, where the jump in temperature leads to a discontinuity of the primal field quantity,

$$[|\Delta T|] = \Delta T^+ - \Delta T^- \neq 0 \tag{47}$$

while the heat flux normal to the interface surface remains continuous if no strong kinematic discontinuity develops.

The Clausius-Duhem inequality in Equation 36 expands for the interface,

$$\boxed{\mathbf{t} : [|\dot{\mathbf{u}}|] - \rho_s \dot{\Psi} - \rho_s s \left[\left|\Delta \dot{T}\right|\right] - \tfrac{q_n \cdot [|\Delta T|]}{\Delta T} \geq 0} \tag{48}$$

we deduce the heat transfer inequality,

$$\frac{q_n \cdot [|\Delta T|]}{\Delta T} \leq 0 \tag{49}$$

which is satisfied by a convective heat transfer condition across the interface surface when $k_{nn} \rightarrow h_c$,

$$\boxed{q_n = -k_{nn} [|\Delta T|] \rightarrow -h_c [|\Delta T|]} \tag{50}$$

Recalling the definition of the local heat capacity:

$$c_s = -[1-d] \frac{\partial^2 \Psi}{\partial [|\Delta T|])^2} \tag{51}$$

we obtain the local equation of heat balance from the first law of thermodynamics:

$$\boxed{\rho_s c_s \left[\left|\Delta \dot{T}\right|\right] + q_n = Q_T - \kappa(\mathbf{t} \cdot [|\dot{\mathbf{u}}|])} \tag{52}$$

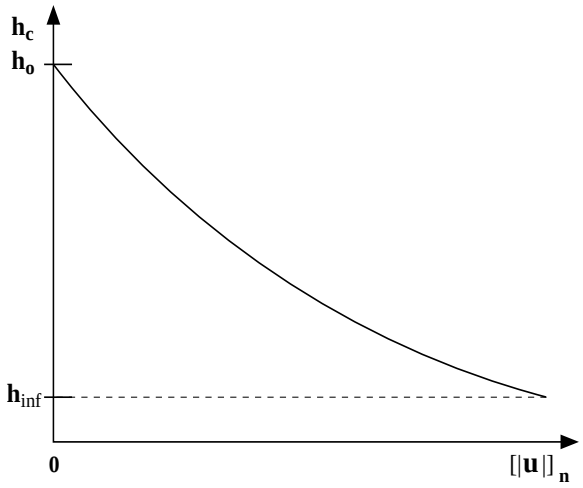

Figure 6: Degradation of convective heat transfer coefficient across zero-thickness interface

where Q_T denotes the heat sources in the interface and where $\kappa \leq 1$ denotes the conversion factor of mechanical energy into heat.
Heat transfer across an opening interface is governed by the convective interface condition:

$$q_n = -h_c\,[|\Delta T|] \tag{53}$$

which varies between $\ell_{el} k_{nn} \geq h_c \geq h_{inf}$ depending on the separation of the interface shown in Figure 6. Hereby h_{inf} denotes the convective heat transfer coefficient for an open crack and $h_o = \ell_{el} k_{nn}$ the thermal conductivity across the closed interface.

For steady state conditions the heat balance reduces to,

$$\boxed{h_c\,[|\Delta T|] = -Q_T + \kappa(\mathbf{t}\cdot[|\dot{\mathbf{u}}|])} \tag{54}$$

where the mechanical and thermal heat sources on the right hand side are normally neglected. This results in a thermal barrier condition across the interface which depends on the strength of the convective heat transfer coefficient h_c.

5 INCLUSION PROBLEM

To illustrate the effects of internal and external restraints we consider the simple model problem of a circular inclusion embedded in a cement matrix. This permits us to examine the fundamental aspects of heterogeneity in a thermal environment when mismatch of thermal expansion and the elastic stiffness leads to differential slip along the interfacial transition zone of the two materials and subsequent damage in the cement matrix. For the sake of argument we assume a unit 2-D domain, $100\,mm \times 100\,mm$ in a state of plane stress. The contrast ratios of the elastic stiffness are $E_m : E_a = 1 : 3$, with $E_m = 25GPa$, $E_a = 75GPa$, and thermal expansion $\alpha_m : \alpha_a = 15 : 9$, with $\alpha_m = 15.0 \times 10^{-6}$, $\alpha_a = 9.0 \times 10^{-6}$. The unstructured mesh of three node CST elements in the cement matrix are connected by four node interface elements with the cohesive strength $f_t = 6\,MPa$ and the fracture energy release rate for interface separation $G_f^I = 0.22\,N/mm$. The initial width of the elastic interface is $\ell_{el} = 10^{-3}\,[mm]$ in relation to the elastic matrix stiffness while the initial characteristic length of the fracture process zone is $\ell_{ch} = 153\,[mm]$.

Assuming that the two-phase assembly is subjected to a temperature raise $\Delta T = T - T_o = 50^o C$ we examine two limiting cases: (a) thermal expansion and mismatch stresses for the case of no external restraint, and (b) thermal expansion and thermal stresses for the case of full external restraint. In both cases a state of plane stress with $\nu = 0.2$ determines the in-plane response which adheres to symmetry boundary conditions along the x-y axes. This infers that we actually analyze the upper right quadrant of an assembly comprised of four inclusions.

5.1 *Thermoelastic Response with no External Restraint*

Figure 7 illustrates the undeformed and the deformed mesh of the two-phase assembly. The thermal expansion of the mortar matrix dominates the overall expansion of the two-phase composite which is magnified by the factor 200. It also exhibits a contraction of the inclusion due to the internal restraint leading to crack opening along the interfacial transition zone and along several interfaces in the mortar matrix.

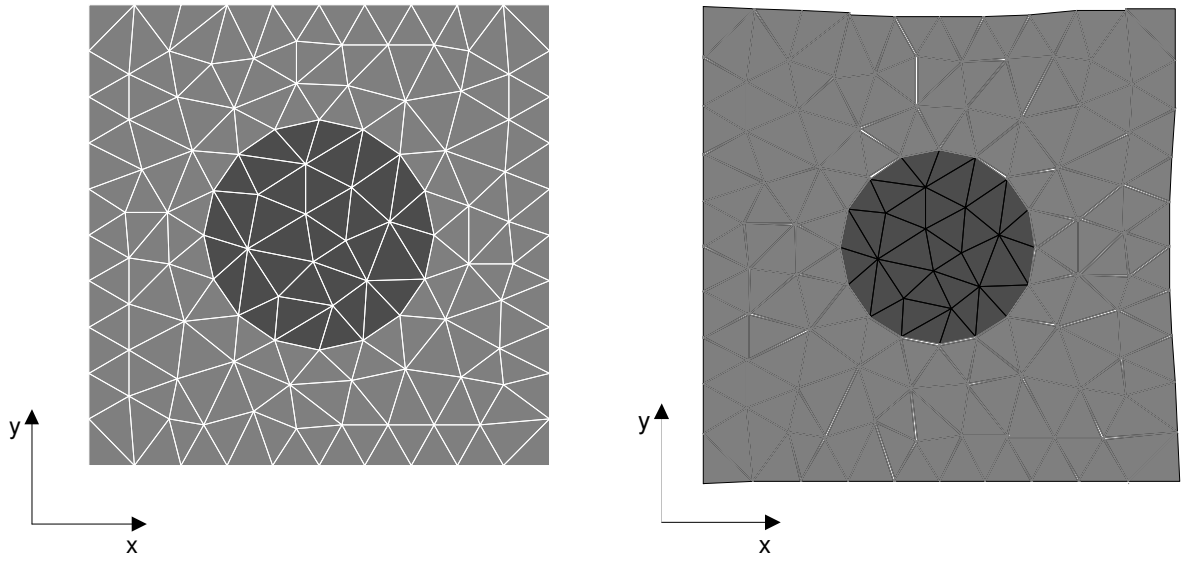

Figure 7: Inclusion problem (without external restraint): (a) undeformed, (b) deformed mesh

Figure 8 shows the distribution of volumetric and deviatoric von Mises stresses in the two constituents. Note that the thermoelastic mismatch leads to significant stress levels reaching nearly the level of tensile strength of the interface layer and a quarter of the thermal stress level in the fully restrained case. In other terms, the internal restraints of the heterogeneous model problem induce stress levels which would normally be zero in the homogeneous case using equivalent material properties. Also note that the state of stress in the elastic inclusion is uniform according to Eshelby, and that the largest shear stresses are concentrated along the interfacial transition zone. We conclude, that the thermoelastic mismatch introduces considerable stress levels which are omitted from consideration if the heterogeneous material structure of the two-phase particle composite is not included.

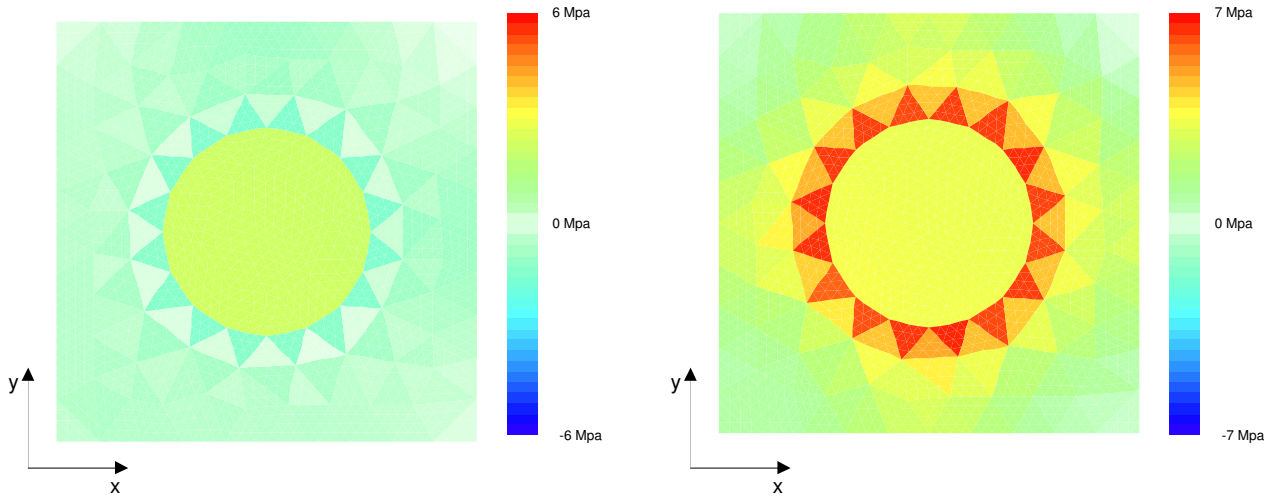

Figure 8: Inclusion problem (without external restraint): (a) volumetric, (b) von Mises stress

5.2 *Thermoelastic Response with full External Restraint*

Figure 9 illustrates the undeformed and the deformed mesh of the assembly subject to full external restraints. In this case the thermoelastic effect of the inclusion dominates the overall deformation of the two-phase composite which is magnified by the factor 200. It exhibits swelling of the inclusion which is caused by the three-fold stiffness of the aggregate leading to extensive crack opening along the interfacial transition zone and along all interfaces in the mortar matrix.

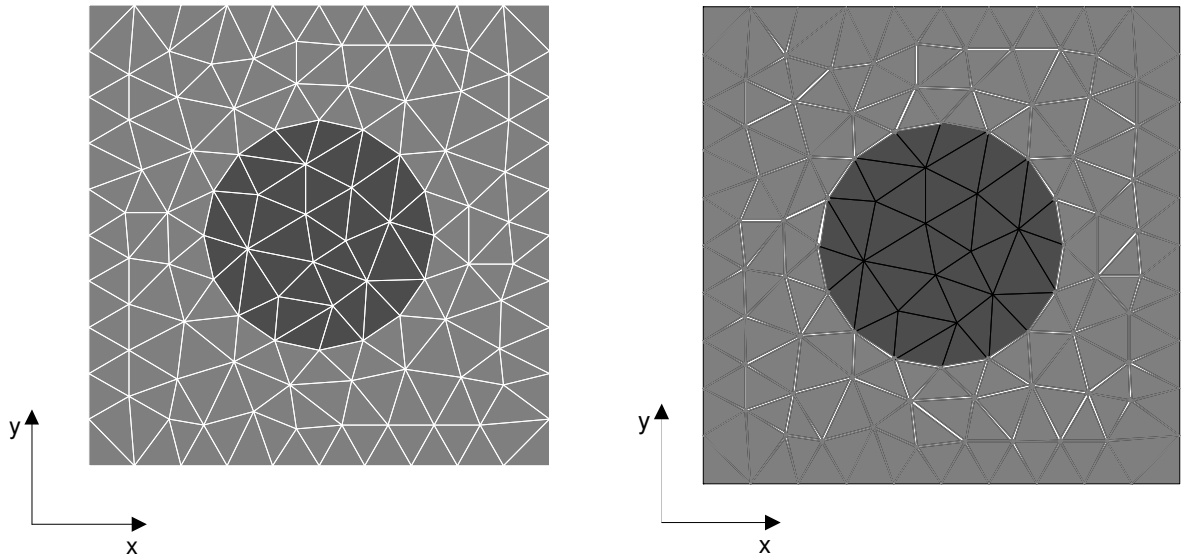

Figure 9: Inclusion problem (with full external restraint): (a) undeformed, (b) deformed mesh

Figure 10 shows the distribution of volumetric and deviatoric von Mises stresses in the two constituents. We observe that the external restraints lead to significant thermal stress levels especially in the

aggregate inclusions because of the three-fold value of their stiffness. Recall that the interface cohesion and shear stresses are only limited by $f_t = 6\,MPa$ in tension but not in compression, and that biaxial compression may induce considerable deviatoric stress levels in the case of plane stress. Note again the uniform state of stress in the elastic inclusion which fully agrees with the analytical result of Eshelby for ellipsoidal inclusions.

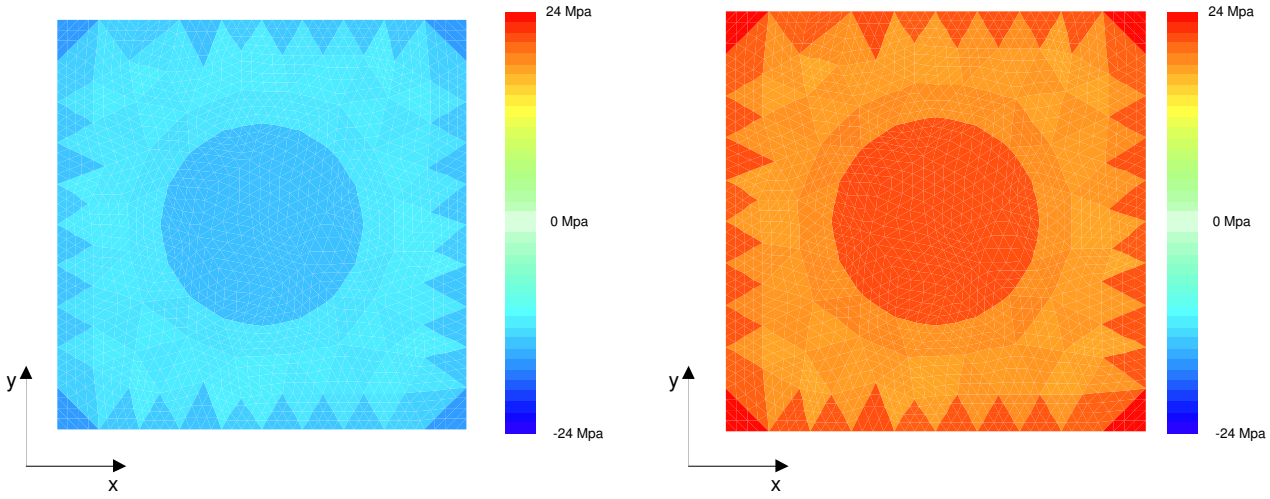

Figure 10: Inclusion problem (with full external restraint): (a) volumetric, (b) von Mises stress

6 TRANSIENT THERMOMECHANICAL DAMAGE PROBLEM

The performance of cement-based materials under elevated temperatures are very complicated and difficult to characterize. With increasing temperature there is a decrease of compressive strength, density, thermal conductivity, thermal diffusivity in concrete because of increase of porosity and permeability [Anderberg and Thelandersson, 1976, 1987; Schneider 1988; Khoury & Sullivan & Grainger 1985; Bazant & Chern 1987, Phan 1996; Bazant & Kaplan 1996]. These changes of physical properties are caused by three processes taking place at elevated temperatures:

(a) Phase transformation processes - Loss of free water occurs at about 100 ^{o}C. Decomposition of calcium hydroxide takes place at about 450 ^{o}C. The crystal structure of quartz transforms at 573 ^{o}C from α- to β- form.

(b) Evolution processes in pore structure - the volume and surface of pores increase up to a temperature of approximately 500 ^{o}C, and decrease with further increase of temperature. Chemical processes result in changes of the pore pressure which affects the pore structure of concrete and thus the permeability and diffusivity.

(c) Coupled thermo-hygro-chemo-mechanical processes - The thermo-mechanical coupling is associated with the temperature gradient upon rapid heating causing severe thermal stress in concrete leading to dehydration and shrinkage of the cement matrix. The thermo-hygral coupling is associated with multiphase transport of water in the liquid, moisture in the vapor, and air in the gaseous phases.

In addition to the thermal softening of the elastic stiffness properties, it is the interaction of the thermal expansion with the mechanical damage which leads to the dramatic reduction of axial stress when confined concrete specimens are subjected to high temperature sweeps $20 \leq T \leq 800^0 C$. Figure 11 which has been reproduced from Anderberg & Thelandersson [1976, 1987] illustrates the dramatic effect of axial restraint on the thermal stress when the temperature in the concrete sample is increased to very high levels and when spalling leads to sometimes explosive failures. Figure 12 shows the effect of axial loading on the thermal expansion of the concrete test article indicating that the free thermal expansion reverts to contraction under the presence of axial compression.

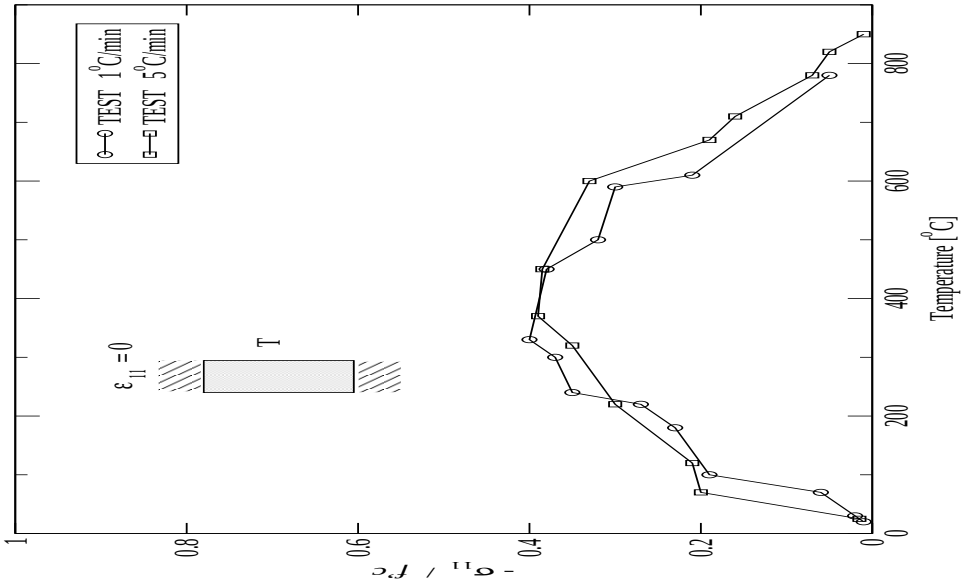

Figure 11: Axial stress in restrained concrete specimen subject to temperature sweep [Thelandersson, 1986]

Clearly, these experiments exhibit time dependence and inelastic processes, different aspects of which were discussed recently by a number of authors [Ulm et al , 1999, Schrefler et al, 2002, Nenech et al, 2002]. However, we believe that the interdependence of thermal and mechanical damage is a very important effect which needs to be addressed, especially when transient high temperature excursions are considered.

As a model problem we consider the two-phase composite in Figure 13 following the meso-mechanical failure studies of concrete by Willam et al [1990]. The 2-D representative volume element (RVE) of size $14\,mm \times 14\,mm$ is subjected to a transient temperature sweep considering mechanical and thermal degradation. The objective of the exercise is to explore the effect of temperature dependence of the mechanical and thermal properties and to compare the numerical results with the experimental observations of Anderberg & Thelandersson [1976, 1987] in Figures 11 and 12. The plane stress study permits us to investigate the interaction of the thermal and mechanical degradation due to interface damage, and to compare the thermal stress response with the results of a continuum damage approach reported by Willam, Inkyu and Xi [2003].

In this model problem mechanical degradation is localized along the interfaces which are inserted among all bi-material surfaces and between most of the matrix-matrix solid elements as illustrated in

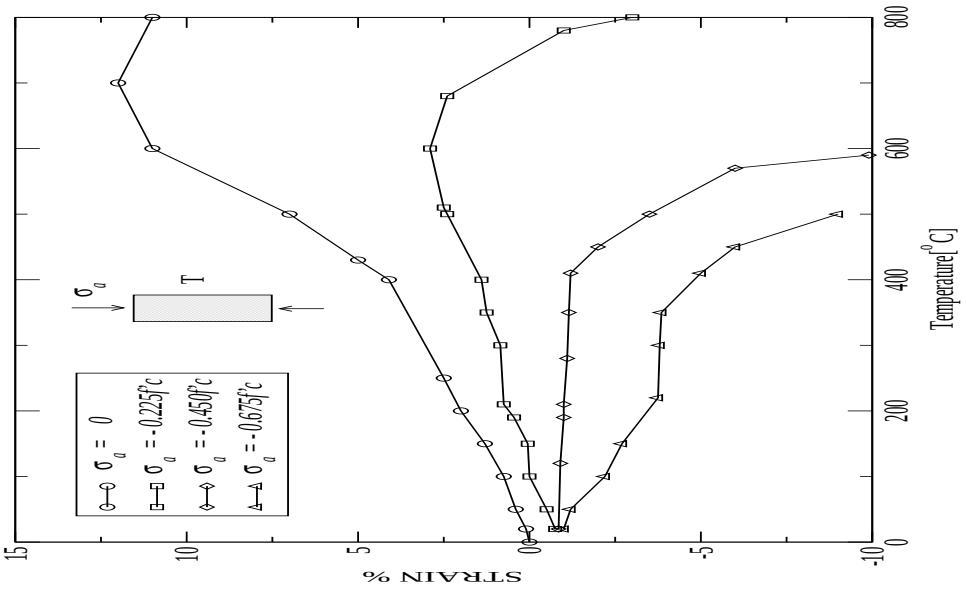

Figure 12: Axial strain in concrete specimen subject to temperature sweep at different confinement levels σ_a [Thelandersson, 1986]

the right inset of Figure 13. The interface properties are the same irrespective whether they represent bi-material adhesion or mono-material cohesion. The solid elements consider temperature effects on the elastic properties and the coefficient of thermal expansion differently for aggregate inclusions and the cement matrix.

The thermal stress analysis is carried out with the explicit time marching strategy outlined in the Appendix. This staggered format decouples the heat transfer analysis from the mechanical degradation analysis. Thereby, the Gough-Joule effect of mechanical cooling is neglected in the heat balance equation, however the crack opening of the interfaces is considered in the form of the convection coefficient which controls heat transfer across the interface as detailed previuosly.

6.1 *Solid Material Properties*

The thermoelastic properties of the solid elements in the cement matrix and aggregate inclusions are listed below:

- Coefficient of Thermal Expansion:

  Cement Matrix : α_m^0=15.5 $\times$ 10^{-6} /C, and α_m= 0.00555557α_m^0(200-T)
  Aggregate Inclusions : α_a^0=9.0 $\times$ 10^{-6} /C and α_a=α_a($e^{0.05T/100}$-0.01)
  Figure 13 illustrates the effect increasing expansion with increasing temperature for the aggregate. The thermal expansion of the cement matrix was modified to include the effect of drying shrinkage. This results in an overall decrease of the coefficient of expansion with increasing temperature as indicated in Figure 14.

- Temperature Dependence of Elastic Modulus:

  E=E_0(0.03921+$e^{-0.002T}$) with E_m=25 GPa, E_a=75 GPa.

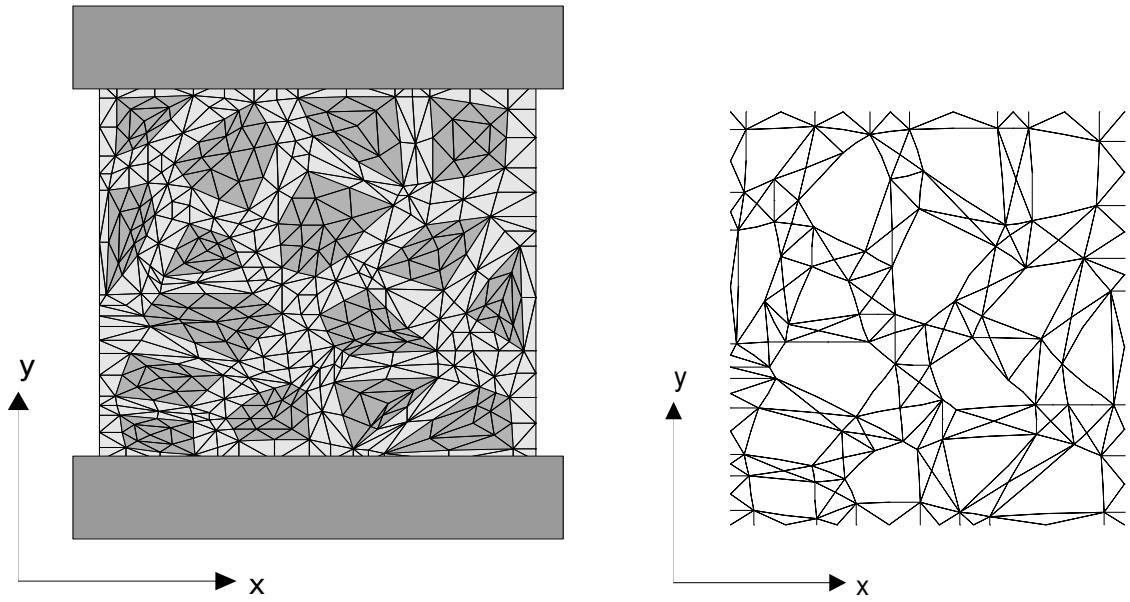

Figure 13: Finite element mesh of RVE and interface layout

Figure 15 illustrates the degradation of the elastic stiffness properties with increasing temperature. Thereby it is assumed that Poisson's ratio exhibits little temperature sensitivity, ν_m=ν_a=0.2.

The heat transfer properties of the solid elements in the cement matrix and aggregate inclusions are listed below:

- Aggregate Inclusions:

  Thermal conductivity, k_a = 2.4 $\times$ 10^{-3} kW/(mm·C), Convection coefficient, h_a = 0.0 kW/(mm^2 ·C), Specific heat, c_a = 1170 (kW · h)/(kg ·C), Mass density, ρ_a = 1.92 $\times$ 10^{-6} kg/mm^3.

- Cement Matrix:

  Thermal conductivity, k_m = 10^{-4} kW/(mm·C), Convection coefficient, h_m = 2$\times 10^{-5}$ kW/(mm^2 ·C), Specific heat, c_m = 1170 (kW · h)/(kg ·C), Mass density, ρ_m = 1.92 $\times$ 10^{-6} kg/mm^3.

6.2 *Interface Material Properties*

For the sake of simplicity all interface properties are assumed to be the same irrespective whether they connect matrix-matrix, inclusion-inclusion or matrix-inclusion elements.

- Mechanical Interface Properties:

  The initial interface stiffness is $k^o = 10 \times 10^3$ GPa/mm which corresponds to a characteristic interface length of $l_{el} = 10^{-3}\, mm$. The cohesive strength is assumed to correspond to the tensile strength of concrete materials f_t=6 MPa, and the fracture energy release rate is G_f^I=0.25 N/mm. The damage evolution follows the exponential growth function in Equations 16 which has been incorporated into the thermomechanical damage model, Equation 44, assuming different values of $b = 0.1, 0.5, 1.0$ in the expression of the equivalent thermodynamic force.

- Heat Transfer Interface Properties:

  The convective heat transfer coefficient is initially for full contact $h_o = 0.1$, while the asymptotic value is for full crack opening $h_\infty = 0.2 \times 10^{-4}$.

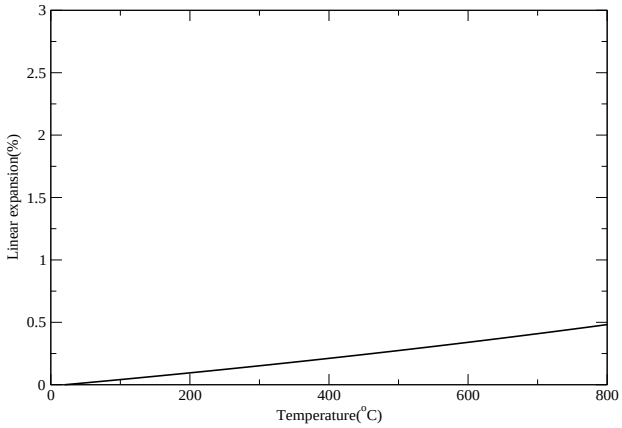

Figure 14: Coefficient of thermal aggregate expansion [%]

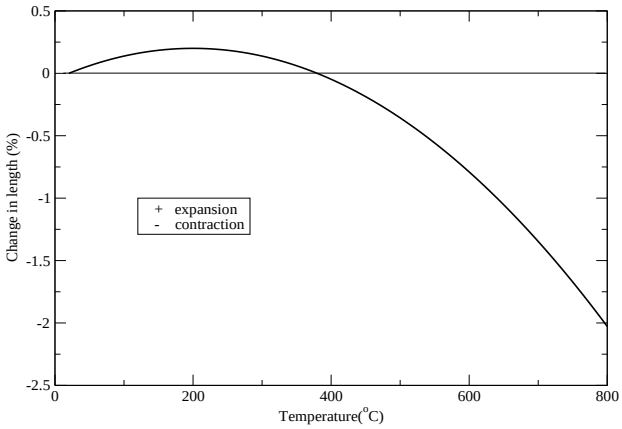

Figure 15: Coefficient of thermal matrix expansion [%]

6.3 *Thermal Sweep Analysis of Two-Phase RVE*

The main results of the thermal sweep analysis are shown in Figures 17, 18, 19 and 20. At the left, the figures depict the distribution of the convective interface heat transfer coefficient which provides a measure of interface opening. At the right, the figures illustrate the axial stress distributions when the ambient temperature reaches $\Delta T = 200, 400, 600, 800^o$ C. The figures show the heterogeneous effects of the aggregate inclusions and the build up of axial compression σ_{yy} in the center region of the RVE, while

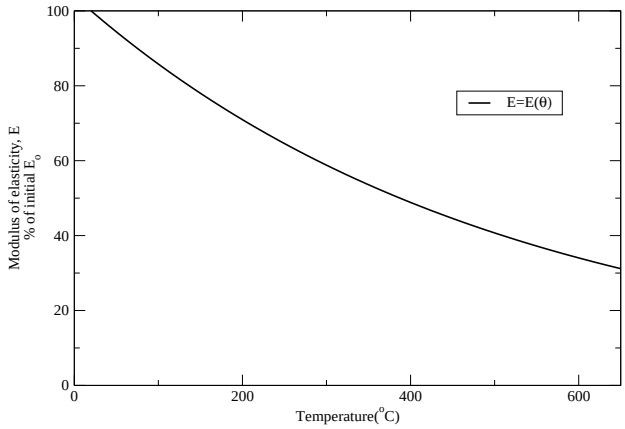

Figure 16: Reduction of elastic modulus with rising temperature, $E = E(T)$

the cement matrix near the midheight of the outside surfaces exhibits tension indicating the tendency of cracking and spalling.

Figure 21 shows the influence of the convective heat transfer coefficient on the temperature distribution in the RVE resulting in a high concentration of temperature gradients along the outside surfaces similar to a thermal barrier for low values of h_c.

The deformed mesh in Figure 22 illustrates the diagonal shear failure mode and the lateral expansion of the deformed mesh (30-fold magnification), when the ambient temperature reaches $\Delta T = 500^o$. The prevalent degradation of mechanical cohesion introduces slip and crack opening primarily at the bi-material interfaces forming a diagonal failure mechanism across the two-phase composite (the results are shown for the friction ratio $b = 1.0$ with equal normal to tangential energy interaction).

The interface damage leads to an overall release of the axial thermal stress depicted in Figure 23. This figure illustrates the axial thermal stress σ_{yy} near the top left corner of the restrained RVE specimen. It compares the predictions of different normal to tangential degradation ratios $b = 0.1, 0.5, 1.0$ with the results of a volumetric-deviatoric damage model without interfaces, see Willam, Rhee and Xi [2003]. Increasing values of the fracture energy ratio b activate tangential damage and reduce the thermal stress effects which reach a maximum value when the ambient temperature approaches $\Delta T = 300^o$. The trends of interface damage are similar to those of the continuous damage model considering volumetric and deviatoric degradation due to thermal and mechanical damage. They reproduce rather well the overall reduction of axial load resistance with increasing temperature and the reversal of axial thermal stress shown in the experiment, see Figure 11.

7 CONCLUSIONS

The paper addressed model issues of zero-thickness cohesive-frictional interfaces which are subjected to thermal and mechanical damage. The damage model, which incorporates degradation in the normal and tangential components, captures degradation effects in heterogeneous media. The two model problems indicate significant stress levels in heterogeneous composites due to thermal mismatch and the prevalent reduction of thermal stress under high temperature sweeps down to nearly zero resistance at $T = 800^o$. The combination of both thermal and mechanical degradation mechanisms is the principal feature which drives the reduction process of axial thermal stress.

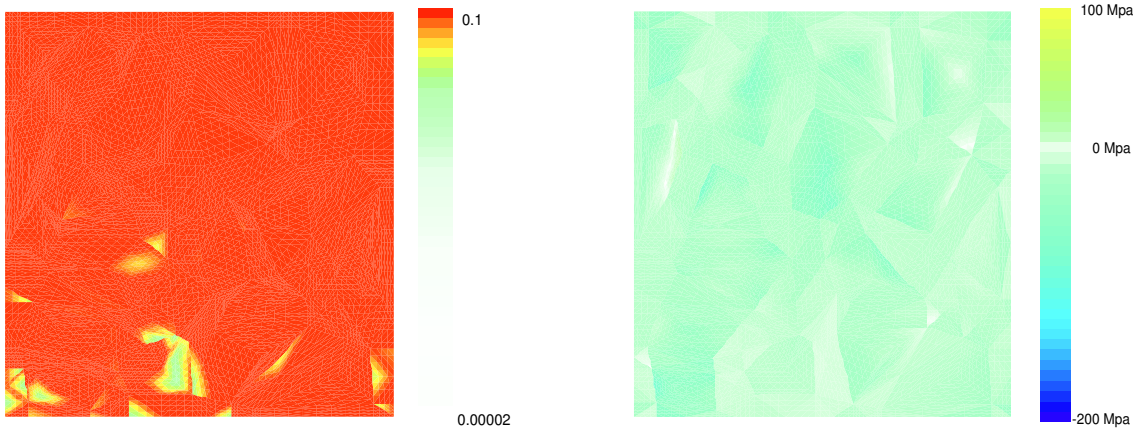

Figure 17: Distribution of interface convection h_c and σ_{yy} contours at ambient temperature=200^oC

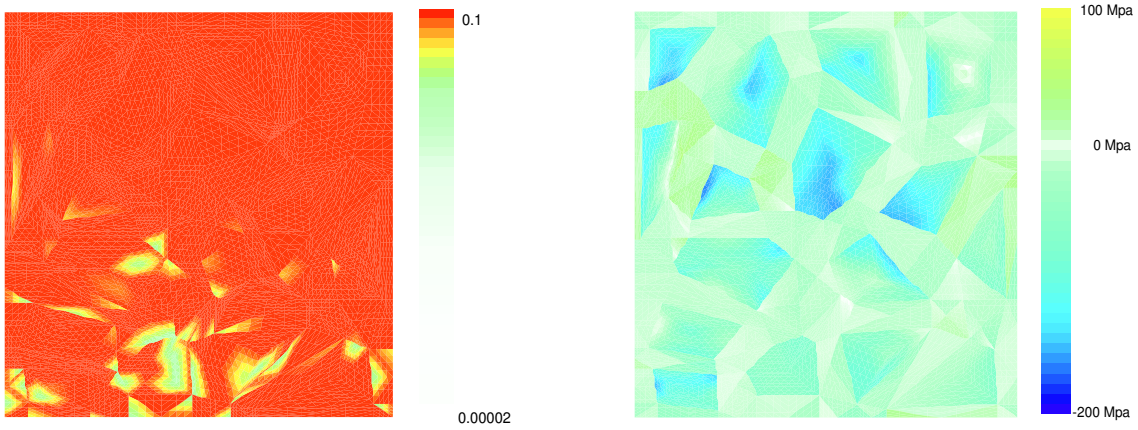

Figure 18: Distribution of interface convection h_c and σ_{yy} contours at ambient temperature=400^oC

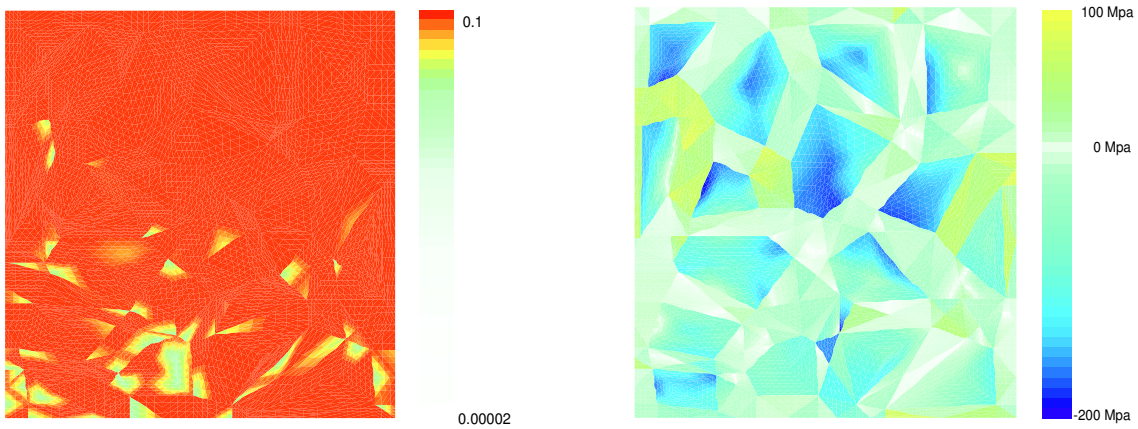

Figure 19: Distribution of interface convection h_c and σ_{yy} contours at ambient temperature=600^oC

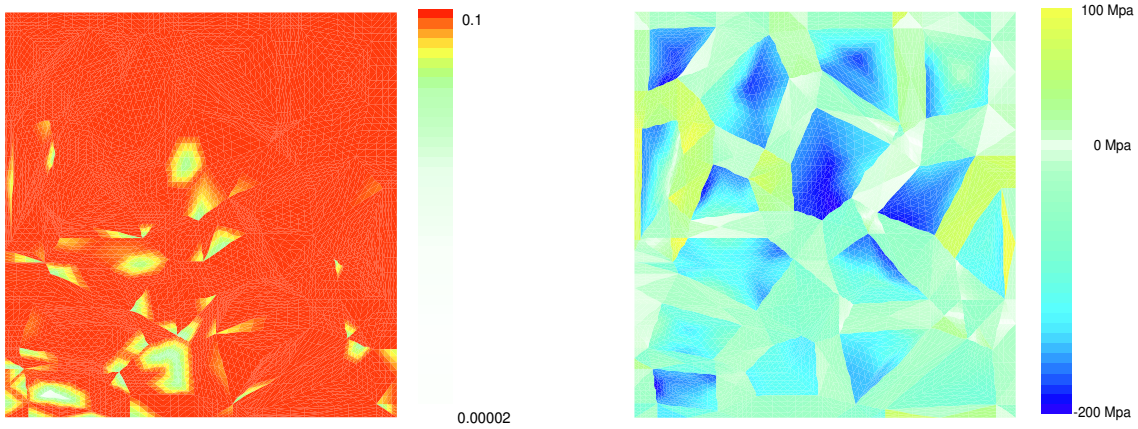

Figure 20: Distribution of interface convection h_c and σ_{yy} contours at ambient temperature=800^oC

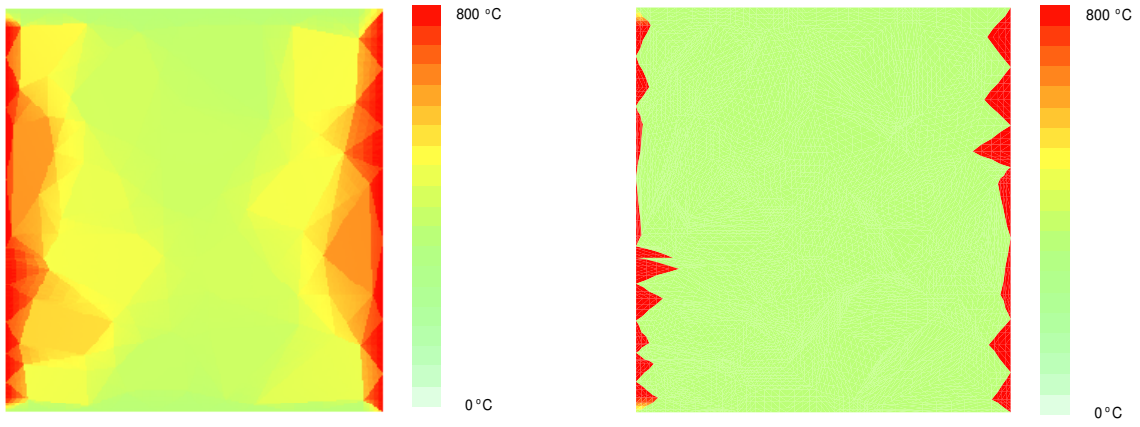

Figure 21: Temperature Distribution: convective interface heat transfer(a) $h_c = 0.0001kW/mm^2C$, (b)$h_c = 0.00001kW/mm^2C$

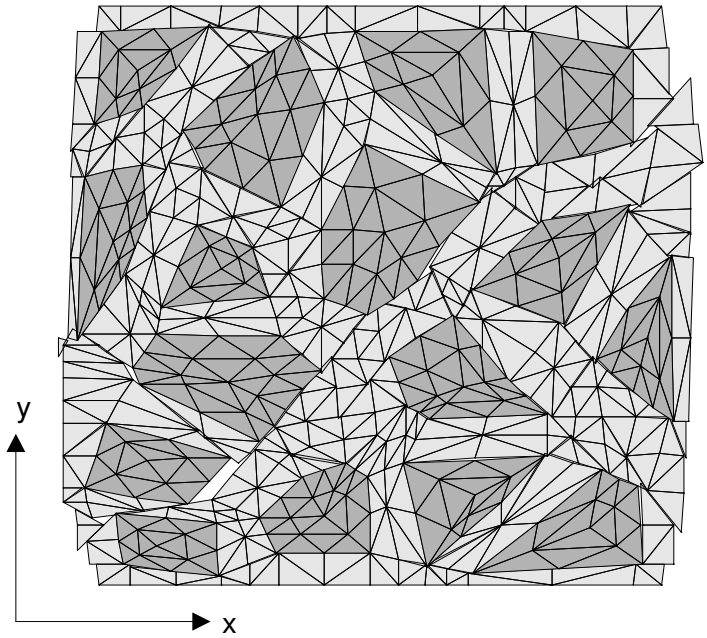

Figure 22: Deformed mesh at ambient temperature=500^oC, 30-fold magnification

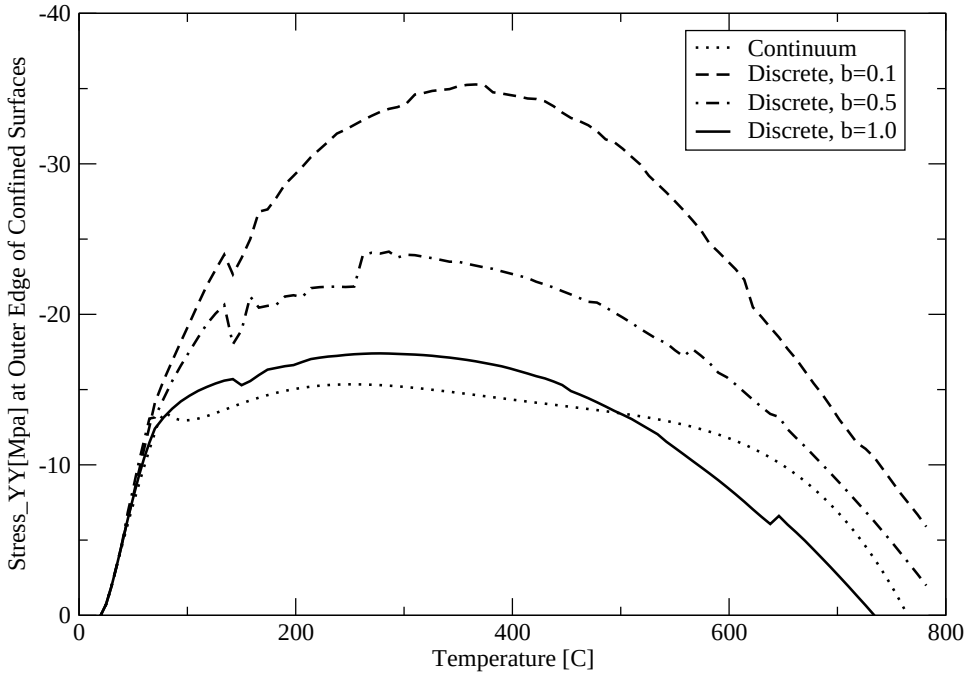

Figure 23: Axial thermal stress results of continuum and discrete damage analyses

8 ACKNOWLEDGEMENTS

This material is based upon work supported by the National Science Foundation under Grant No. 0084598. The authors wish to acknowledge support of the exploratory project: *Simulation Platform for the Earthquake Response of Reinforced Concrete Structures*.

REFERENCES

Anderberg, Y. and J. Thelanderssson (1976). Stress and deformation characteristics of concrete at high temperatures. Technical report, Lund Institute of Technology, Lund, Sweden.

Bazant, Z. and J.-C. Chern (1987). Stress-induced thermal shrinkage strain in concrete. *Journal of Engineering Mechanics, ASCE 113*(10), 1493–1511.

Bazant, Z. and M. Kaplan (1996). *Concrete at High Temperatures, Material Properties and Mathematical Models*. Burnt Mill, England: Longman Group Limited.

Brewer, J. and P. Lagace (1988). Quadratic stress criterion for initiation of delamination. *Journal of Composite Materials 22*, 1141–1155.

Camacho, G. and M. Ortiz (1996). Computational modeling of impact damage in brittle materials. *International Journal of Solids and Structures 33*, 2899–2938.

Carol, I., P. Prat, and C. López (1997). A normal/shear cracking model. Application to discrete crack analysis. *Journal of Engineering Mechanics, ASCE 123*(8), 765–773.

Carol, I., E. Rizzi, and K. Willam (2002). An 'extended' volumetric/deviatoric formulation of anisotropic damage based on a pseudo-log rate. *European Journal of Mechanics -A/Solids 21*, 747–772.

Corigliano, A. and O. Allix (2000). Some aspects of interlaminar degradation in composites. *Computer Methods in Applied Mechanics and Engineering 185*, 203–224.

Desai, C. (2001). *Mechanics of Materials and Interfaces: The Disturbed State Concept*. Florida: CRC Press, Boca Baton.

Espinosa, H. and P. Zavattieri (2003). A grain level model for the study of failure initiation and evolution in polycrystalline brittle materials part i: Theory and numerical implementation. *Mechanics of Materials*, —.

Gens, A., I. Carol, and E. Alonso (1990). An interface element formulation for the analysis of soil-reinforcement interaction. *Computers and Geotechnics 7*, 133–151.

Hillerborg, A., M. Modeer, and P. Petersson (1976). Analysis of crack formation and crack growth in concrete by means of fracture mechanics and finite elements. *Cement and Concrete Research 6*(6), 773–782.

Kachanov, L. (1958). Time of the rupture process under creep conditions. *Izv. Akad. Nauk. S.S.R., Otd, Tekh. Nauk. 8*, 26–31.

Khoury, G., P. Sullivan, and B. Grainger (1985). Transient thermal strain of concrete: Literature review, conditions within specimen and individual constituent behaviour. *Magazine of Concrete Research 37*(132), 131–144.

Lofti, H. and B. Shing (1994). Interface model applied to fracture of masonry structures. *Journal of Structural Engineering, ASCE 120*(1), 63–80.

Nenech, W., F. Meftah, and J. Reynouard (2002). An elasto-plastic damage model for plain concrete subjected to high temperatures. *Engineering Structures 24*, 597–611.

Oliver, X., A. Huespe, M. Pulido, and E. Chaves (2001). From continuum mechanics to fracture mechanics: the strong discontinuity approach. *Engineering Fracture Mechanics 69*, 113–136.

Phan, L. (1996). Fire performance of high strength concrete: A report of the state-of-the-art. Technical report, Building and Fire Research Laboratory, National Institute of Standards and Technology, Maryland.

Rots, J. and J. Schellekens (1990). *Interface elements in concrete mechanics*. Swansea, UK: Computer-aided Analysis and Design of Concrete Structures, N. Bićanić and H. Mang editors, Pineridge Press, pp.909–918.

Schellekens, J. and R. de Borst (1993). On the numerical integration of interface elements. *International Journal for Numerical Methods in Engineering 36*(7), 43–66.

Schneider, U. (1988). Concrete at high temperature - a general review. *Fire Safety Journal 13*(1), 55–68.

Schrefler, B., G. Khoury, D. Gawin, and C. Majorana (2002). Thermo-hydro-mechanical modelling of high performance concrete at high temperatures. *Engineering Computations 19*(7), 787–819.

Simo, J., J. Oliver, and F. Armero (1993). An analysis of strong discontinuities induced by strain-softening in rate-independent inelastic solids. *Computational Mechanics 12*, 277–296.

Stankowski, T., K. Runesson, and S. Sture (1993). Fracture and slip of interfaces in cementitious composites. *Journal of Engineering Mechanics, ASCE 119*(2), 292–306.

Thelandersson, S. (1987). Modeling of combined thermal and mechanical action in concrete. *Journal of Engineering Mechanics, ASCE 113*(6), 893–906.

Tijssens, M. (2000). *On the Cohesive Surface Methodology for Fracture of Brittle Heterogeneous Solids*. Maastricht, The Netherlands: Ph.D. Dissertation TU-Delft, Shaker Publ. B.V.

Ulm, F.-J., P. Acker, and M. Lévy (1999). The *"chunnel"* fire ii: analysis of concrete damage. *Journal of Engineering Mechanics, ASCE 125*(3), 283–289.

Ulm, F.-J., O. Coussy, and Z. Bažant (1999). The *"chunnel"* fire i: chemoplastic softening of rapidly heated concrete. *Journal of Engineering Mechanics, ASCE 125*(3), 272–282.

Willam, K., I. Rhee, and Y. Xi (2003). Thermal degradation in heterogeneous concrete materials. *Journal of Engineering Materials, ASCE 129*, –.

Willam, K., T. Stankowski, K. Runesson, and S. Sture (1990). *Simulation Issues of Distributed and Localized Failure Computations, Proceedings on Cracking and Damage-Strain Localization and Size Effects*. London and New York: Mazars, J. and Bažant, Z. Eds., Elsevier Applied Sciences.

Xu, X.-P. and A. Needleman (1994). Numerical simulations of fast crack growth in brittle solids. *J. Mech. Phys. Solids 42*(9), 1397–1434.